Environmental Science & Technology

pubs.acs.org/est

Article

Emissions of Nitrous Acid, Nitryl Chloride, and Dinitrogen Pentoxide Associated with Automotive Braking

Madeline E. Cooke, Michelia Dam, Lisa M. Wingen, Véronique Perraud, Adam E. Thomas, Berenice Rojas, Sanjeevi Nagalingam, Michael J. Ezell, Samuel La Salle, Paulus S. Bauer, Barbara J. Finlayson-Pitts,* and James N. Smith*

Cite This: *Environ. Sci. Technol.* 2025, 59, 9167−9177

Read Online

ACCESS | Metrics & More | Article Recommendations | Supporting Information

ABSTRACT: As worldwide trends move toward replacing combustion transportation modes with electric vehicles, characterizing non-tailpipe emissions, such as those from brake wear, becomes increasingly important. Nitrous acid (HONO), nitryl chloride ($ClNO_2$), and dinitrogen pentoxide (N_2O_5) are important sources of radical oxidants (e.g., •OH, •Cl, $•NO_3$) and nitrogen oxides (NO_x) in the atmosphere, driving the chemistry that leads to air quality degradation. Discrepancies between measurements and model predictions indicate that there are significant unknown sources of these species, particularly HONO, where the contributions of different formation processes have been controversial since the first ambient observations in the 1970s. We report the generation of these reactive nitrogen species during automotive braking using chemical ionization mass spectrometry configured with iodide reagent ion. Substantial HONO levels are observed from ceramic and semi-metallic brake pads, and smaller quantities of $ClNO_2$ and N_2O_5 were also detected. We propose that HONO is formed in the hot plume emanating from the brake rotor via abstraction by NO_2 of allylic and aldehyde hydrogen atoms found in the complex mixture of volatile organic compounds emitted simultaneously. These results suggest that emissions from automotive braking must be taken into account in urban oxidation chemistry.

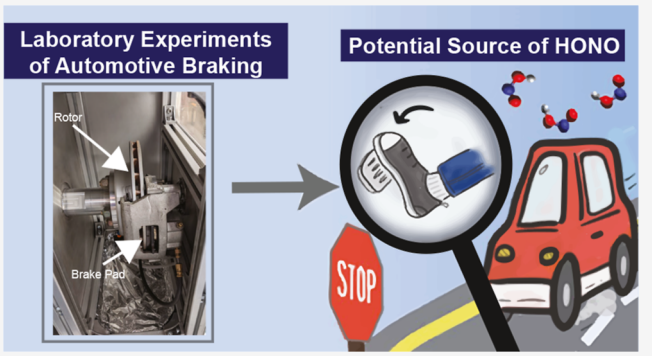

KEYWORDS: *non-tailpipe emissions, chemical ionization mass spectrometry, brake wear, reactive nitrogen species, nitrous acid (HONO)*

INTRODUCTION

Reactive nitrogen species, including nitrous acid (HONO), nitryl chloride ($ClNO_2$), and dinitrogen pentoxide (N_2O_5), are important reservoirs for key radical oxidants (e.g., hydroxyl radicals (•OH), chlorine radicals (•Cl), and nitrate radicals ($•NO_3$)) as well as nitrogen oxides ($NO_x = NO + NO_2$) in the atmosphere.[1] These reactive nitrogen species strongly influence tropospheric chemistry.[2] For example, •OH can be generated through the photolysis of HONO (R1)

$$HONO_{(g)} + h\nu\ (300 < \lambda < 405\ \text{nm}) \rightarrow HO\cdot_{(g)} + NO_{(g)} \quad \text{(R1)}$$

and subsequently react with volatile organic compounds (VOCs) to form peroxy radicals that oxidize NO to NO_2. Photolysis of NO_2 is the sole known anthropogenic source of ozone, an air pollutant which has deleterious health effects, and is itself a key atmospheric oxidant and greenhouse gas.[1] The presence of HONO drives this chemistry forward; in fact, •OH generated through R1 can account for up to 55% of •OH production during the daytime[3−5] and up to 80% of •OH production shortly after sunrise.[6]

Nitryl chloride ($ClNO_2$) and dinitrogen pentoxide (N_2O_5) similarly contribute to tropospheric chemistry. For example, photodissociation of $ClNO_2$ generates •Cl and NO_2 (R2).

$$ClNO_{2(g)} + h\nu\ (300 < \lambda < 405\ \text{nm}) \rightarrow Cl\cdot_{(g)} + NO_{2(g)} \quad \text{(R2)}$$

The highly reactive •Cl also oxidizes organics, accelerating photochemical ozone production,[7] and initiating oxidation processes that lead to the formation of air pollutants such as ozone and secondary organic aerosol particles (SOA).[8,9] Dinitrogen pentoxide influences tropospheric chemistry through its role as a source of $•NO_3$ and as both a reservoir or a sink for atmospheric NO_x. Additionally, its multiphase

Received: November 27, 2024
Revised: April 16, 2025
Accepted: April 17, 2025
Published: April 30, 2025

https://doi.org/10.1021/acs.est.4c13202
Environ. Sci. Technol. 2025, 59, 9167−9177

reactions with chloride on surfaces or in particles forms $ClNO_2$ (R3).[10]

$$N_2O_{5(g)} + Cl^-_{(aq)} \rightarrow ClNO_{2(g)} + NO_3^-{}_{(aq)} \quad \text{(R3)}$$

Despite the major influence that these species have on tropospheric chemistry, the formation mechanisms, heterogeneous chemistry, and sources of HONO, N_2O_5 and $ClNO_2$ in the atmosphere are not yet fully understood.[3,11−16]

For decades, the HONO budget in the atmosphere has remained unresolved. HONO was first unambiguously identified in the ambient atmosphere in the late 1970s.[17,18] Since then, field measurements spanning decades have shown evidence for high HONO levels across the globe in diverse regions including urban (up to 4 ppb),[6,17] forested (up to 1 ppb),[19,20] and coastal environments (up to 3 ppb).[21,22] There are five currently known sources of HONO: direct emissions from combustion processes (e.g., vehicle exhaust or biomass burning),[23,24] the gas-phase reaction of $^{\bullet}OH$ with NO, photochemically driven reactions (e.g., reaction of NO_2 on organic surfaces[25] or photolysis of particulate nitrate),[26,27] biological processes (e.g., emission from soil nitrite)[28−30] and the heterogeneous hydrolysis of NO_2 on surfaces (R4),[31] which is accelerated when catalyzed by TiO_2.[32]

$$2NO_{2(g)} + H_2O_{(adsorbed)} \rightarrow HONO_{(g)} + HNO_{3(adsorbed)} \quad \text{(R4)}$$

HONO levels have been repeatedly shown to build up during the nighttime,[33,34] and then quickly photolyze during the early morning hours. Despite its short lifetime (5−10 min) due to rapid photolysis, HONO levels remain above limits of detection during the daytime, suggesting that there exist constant and significant sources.[21] Vertical gradient measurements show that HONO mixing ratios are highest near the ground surface,[35,36] which has led many to hypothesize that heterogeneous chemistry on surfaces such as soil[37,38] or urban grime[39−41] is a significant formation pathway for HONO. However, neither daytime nor nighttime measured HONO levels can be explained by the current HONO formation processes,[3] indicating that unknown HONO sources remain.

Ambient levels of $ClNO_2$ are generally highest in polluted coastal environments (up to 2 ppb)[7,42] due to the abundance of particulate chloride from marine emissions to undergo multiphase reactions with N_2O_5. During the wintertime, road salt can also act as a source of particulate chloride,[43−45] leading to high $ClNO_2$ levels in urban environments. Interestingly, field measurements in urban environments without a marine source during the summertime have also quantified significant $ClNO_2$ (up to 250 ppt).[46] N_2O_5, the main precursor to $ClNO_2$, is generated from the reaction of $^{\bullet}NO_3$ and NO_2, with the $^{\bullet}NO_3$ generated from the reaction of NO_2 and O_3. Overall, ambient N_2O_5 levels can be quite high, particularly at night (up to 15 ppb).[47] Discrepancies remain between the measured and modeled levels of $ClNO_2$ generated through the reaction of N_2O_5 with chloride to form $ClNO_2$ (R3),[48] indicating that uncertainties remain regarding its formation, such as in the N_2O_5 uptake coefficient,[11−13] or that there remain unknown sources of ambient $ClNO_2$.

Automotive braking is a significant source of particles in urban environments.[49−51] With the national trend toward vehicle electrification, emissions from non-tailpipe automotive sources (e.g., brake or tire wear) are of increasing importance. A wide body of research has been dedicated to characterizing particle-phase emissions from brake wear,[52−61] but much less attention has been paid toward characterizing the composition of gas-phase emissions. A recent study by Perraud et al.[62] identified substantial gaseous emissions, demonstrating that volatile and semivolatile organic compounds as well as NO_x are emitted from braking processes, and a study by Patel et al.[63] showed that these gaseous emissions are reactive to atmospheric photooxidation. In both studies, numerous organic gases were measured, such as phenols and nitrogen-containing organics, and their formation was hypothesized to occur due to the degradation of the organic components of brake pad materials. For example, a main organic component of brake pads is phenolic resins, which act as binding agents.[64,65] In general, gas-phase emissions could originate from thermal processes and/or secondary chemistry from these brake materials, but this remains unclear. To our knowledge, no previous studies have investigated the potential for automotive braking to generate gaseous reactive nitrogen compounds including HONO, $ClNO_2$, or N_2O_5.

We present the first observations of emissions of HONO, $ClNO_2$ and N_2O_5 associated with automotive braking simulated using a custom-built brake dynamometer equipped with two common brake pad types: ceramic and semi-metallic. Two braking conditions were applied, representative of light and heavy braking conditions. Chemical ionization mass spectrometry (CIMS) with iodide reagent chemistry was conducted to unambiguously identify the emission of these reactive nitrogen species. Chemistry between NO_2 and VOC occurring in the hot plume coming off the brake rotor is hypothesized as the source of HONO. Impacts on urban oxidation chemistry are discussed.

MATERIALS AND METHODS

Braking Conditions. A custom-built brake dynamometer was used to replicate automotive braking processes, as has been described previously.[55,62,66] A photo of the dynamometer is provided in Figure 1a. Extensive details on the dynamometer system are provided in the Supporting Information. For these experiments, two brake pad types were selected based on their wide use in passenger vehicles within the United States: ceramic (Kodiak model DBC-225) and semi-metallic (BrakeBest model MKD289). A list of the experiments that are included in this study is provided in Table S1.

The custom-built dynamometer used herein is not capable of accurately simulating real-world driving emissions given that it is operated at a constant rotational speed and thus cannot undergo the typical driving cycles used to estimate vehicular emissions.[67,68] For this reason, emission factors (EF) are not an outcome of this study. Nonetheless, the dynamometer system allowed us to reproducibly achieve braking torque and temperature representative of real-world driving,[67] operated in a step-function manner similar to what has been done previously.[69] Two braking cycles were devised to simulate (1) light braking conditions and (2) heavy braking conditions, typical of passenger vehicles, as previously described by Perraud et al.[62]

An overview of the torque, braking pressures, temperature of the chamber, and temperature of the rotor in a typical experiment (Exp. #1) is provided in Figure 1b,c. For reference, these parameters are provided for the remaining experiments in Figures S1−S3. The temperatures of the rotor and chamber increase throughout the experiment due to heat generated from repeated friction on the brake pads, with the rotor

https://doi.org/10.1021/acs.est.4c13202
Environ. Sci. Technol. 2025, 59, 9167−9177

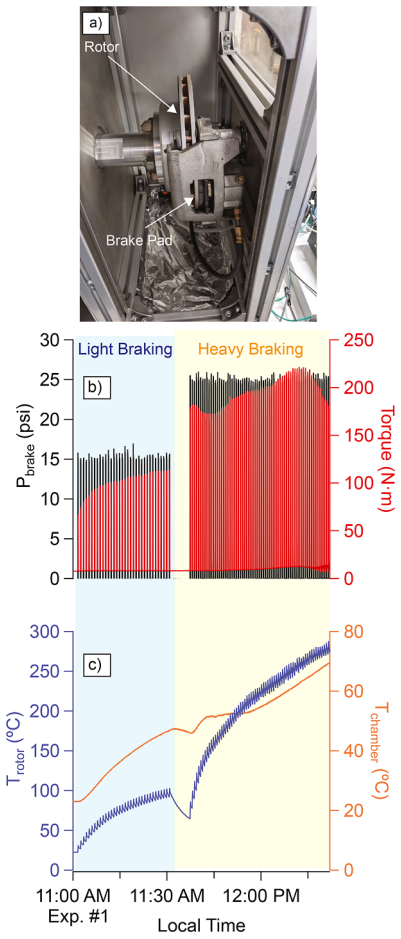

Figure 1. Overview of brake dynamometer and experimental conditions for a representative braking cycle. These data were collected with ceramic brakes. Information includes (a) photo of the dynamometer housed in 87 L chamber, (b) typical brake pressure and torque conditions during cycles of light braking (blue background) and heavy braking (yellow), and (c) rotor and chamber temperature during light and heavy braking cycles.

reaching temperatures up to ~280 °C. Additionally, mixing ratios of NO and NO_2 were continuously measured throughout the braking experiments using a NO_x chemiluminescence analyzer (Thermo Scientific, model 42C). It should be noted that NO_x analyzers based on chemiluminescence measurements have significant interferences from a number of other gas-phase species, notably organic gases (e.g., olefins or alkyl nitrates),[70] which are emitted in abundance during the experiments presented herein. The NO_x measurements in this study were not corrected for these interferences, and thus should be treated as an upper bound for NO_x concentrations. Volatile organic compounds (VOC) levels were monitored in real-time during these experiments using proton transfer reaction mass spectrometry (PTR-MS, Ionicon Analytik, model 8000). During the heavier braking conditions, the emissions from the dynamometer were diluted with various amounts of zero air to prevent saturation of the signals and depletion of the reagent signal. For each experiment, a total equivalent VOC (ppb) concentration was determined using the kinetic method following the procedure described in Perraud et al.[62] Before each experiment, the walls of the chamber surrounding the dynamometer were cleaned to minimize effects due to contamination from previous experiments. Wall losses during experiments were not taken into account.

CIMS Measurements. Gas-phase composition was continuously monitored throughout braking experiments using a high-resolution time-of-flight CIMS (LTOF, Aerodyne Research) configured with iodide reagent chemistry with 1 s time resolution. A 3/8″ Teflon sampling line connected the CIMS directly to the chamber enclosing the braking apparatus. The CIMS was equipped with a custom-built transverse ionization (TI) inlet, as described in detail previously.[71] Briefly, chemical ionization in the TI inlet occurs at ambient temperature and pressure. The TI inlet contains a curtain gas flow of N_2(g) radially applied at the inlet of the mass spectrometer, which maintains a low RH within the inlet and prevents water clusters from forming during chemical ionization. I^- reagent ions were generated by flowing N_2 over Teflon permeation cells containing methyl iodide (99%, stabilized, Acros Organics). The methyl iodide flow was then subsequently directed through a polonium radioactive source (^{210}Po, model P-2021, NRD LLC) to generate I^- before entering the CIMS inlet. Details for analysis of CIMS results including mass calibration, background subtraction, and flow normalization are provided in the Supporting Information.

CIMS Calibrations. CIMS calibrations were performed for the reactive nitrogen species included in this study (HONO, $ClNO_2$, and N_2O_5), and a detailed description of the calibration procedure is included in the Supporting Information. Briefly, an online system was utilized to generate HONO for calibration,[72,73] and a diagram of this system is provided in Figure S4. The stability of the HONO generator was confirmed by triplicate control experiments (Figure S5). The mixing ratio of the stable HONO outflow from the generator was determined using Fourier Transform Infrared (FTIR) spectroscopy to be 8.9 ± 0.5 ppm from these control experiments (Figure S6). The outflow of the HONO generator was diluted with zero air (model 747-30, Aadco Instruments) before entering the CIMS inlet to achieve a wide calibration range, the details of which are provided in Table S2.

N_2O_5 and $ClNO_2$ were synthesized offline for CIMS calibration, and the details of the synthesis procedures are provided in the Supporting Information. CIMS calibrations were conducted by preparing a 5 L bulb with a known mixing ratio of the analyte gas ($ClNO_2$ or N_2O_5) in air (Praxair, Ultrazero grade). Similar to the calibration with HONO, the analyte flow downstream from the bulb was diluted with zero air before entering the CIMS inlet to achieve a wide calibration range. Details regarding the calibration procedure and a diagram of the calibration setup (Figure S7) are provided in the Supporting Information. The CIMS signal was corrected for decay of the analyte within the bulb during the calibration process, an example of which is provided in Figure S8. The range of dilution flows, corresponding N_2O_5 or $ClNO_2$ mixing ratios, and resulting $I(N_2O_5)^-/I^-$ or $I(ClNO_2)^-/I^-$ are provided in Tables S3 and S4, respectively.

The CIMS was calibrated for a wide range of HONO, N_2O_5, and $ClNO_2$ mixing ratios (Figure S9), and a linear response was observed for all three species ($r^2 > 0.9$). The sensitivity of CIMS for these species differs by several orders of magnitude. For direct comparison, the linear relationship of N_2O_5 and $ClNO_2$ is plotted on the same graph in Figure S10. The greatest response factor was observed for N_2O_5, which agrees with previous research showing that N_2O_5 is ionized by I^- at the collision limit.[74]

https://doi.org/10.1021/acs.est.4c13202
Environ. Sci. Technol. 2025, 59, 9167−9177

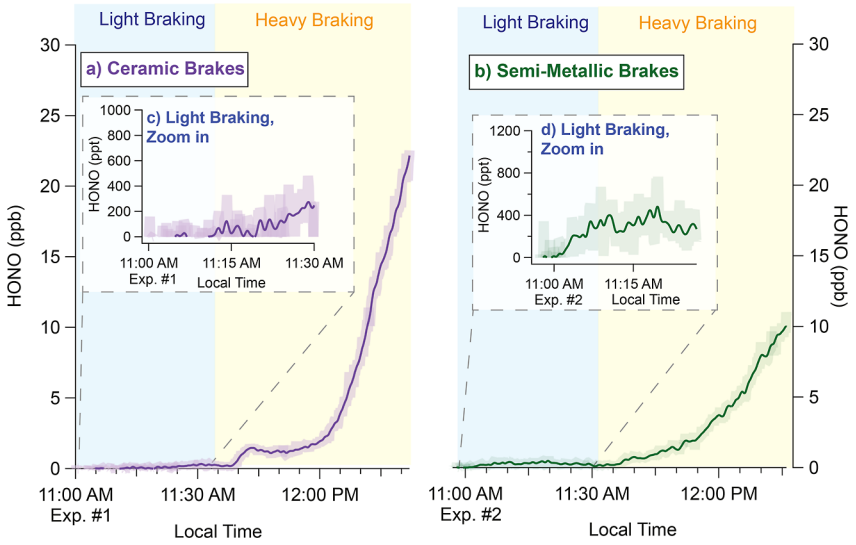

Figure 2. HONO levels during (3a) ceramic and (3b) semi-metallic braking experiments. Period of light braking is highlighted in blue and period of heavy braking is highlighted in yellow. Inset shows an expanded view of the HONO levels during light braking conditions (3c and 3d), with the quantification shown in units of ppt. Line on graphs represents smoothed results and shaded region represents the variation over ∼2 min average of CIMS collection.

Control Experiments of HONO Formation from Secondary Reactions. To investigate the potential for HONO generation to occur through secondary processes, organic gases from a multicomponent calibration mixture as well as from brake emissions were reacted with NO_2 in a separate series of experiments. The details for these experiments are provided the Supporting Information, including the composition of organic gases (Tables S5 and S6). Briefly, organic gases were collected during heavy braking with both ceramic and semi-metallic brake pads using sorbent tubes packed with Tenax TA and Carbograph 5TD (Markes International, Inc.). In offline experiments, these gases were desorbed into a 5 L glass bulb and reacted with NO_2 in excess (277 ppm) over the temperature range 65 to 76 °C, the highest accessible temperature in this apparatus. The high concentration of NO_2 was necessary to see if it was possible to form HONO by reactions with VOC even at the lower temperatures associated with light braking. The formation of HONO in the bulb was followed before and after introduction of the VOC.

RESULTS AND DISCUSSION

HONO from Braking. HONO mixing ratios were determined for both ceramic and semi-metallic brake pads during light and heavy braking conditions (Figures 2a,b and S11a,b). The amount of HONO measured depended on the composition of the brake pads, braking force applied, and temperature. During light braking conditions, the maximum HONO levels were greater for semi-metallic than for ceramic brake pads (Figures 2 and S11), potentially due to the higher temperatures reached during light braking with semi-metallic brake pads (Figures S1 and S3). The dynamics of HONO formation were also dependent on the type of brake pad. During light braking conditions, the amount of HONO began to increase in the chamber nearly immediately when using semi-metallic brakes, but only increased after ∼10 min of braking for ceramic brake pads (Figures 2c,d). These dynamics were found to be consistent in duplicate experiments, the data for which are provided in Figure S11.

Overall, much higher levels of HONO were observed during heavy braking conditions. For heavy braking, greater HONO levels were measured from ceramic brakes than semi-metallic (Figures 2 and S11). The dynamics of HONO formation were again dependent on brake pad type. The rate of increase in measured HONO levels during heavy braking was smaller for the semi-metallic compared to the ceramic brakes. For ceramic brake pads, HONO initially increased to a plateau after ∼7 min of heavy braking and then rapidly increased until braking was stopped. For semi-metallic brakes, HONO steadily increased over the course of the heavy braking experiment.

A key difference between the heavy and light braking conditions is the magnitude of the temperature of both the rotor, T_{rotor}, and the chamber, $T_{chamber}$ (Figures 1c, S1b, S2b, and S3b). Overall, higher $T_{chamber}$ and T_{rotor} conditions were reached during the heavy braking conditions for both ceramic and semi-metallic brake pads, trending with the greater HONO levels during heavy braking, as shown in the color scales of Figures S12−S15. After braking stopped, HONO levels dropped immediately, but $T_{chamber}$ and T_{rotor} remained high for several minutes, suggesting that emissions due to friction processes may play a role in HONO formation.

In addition to HONO, NO and NO_2 levels increased during the experiments, indicating that NO_x is formed during braking processes as shown previously by Perraud et al.[62] and presented in Figure S16. The relationship between HONO and NO_2 during the heavy braking experiments was explored, including the ratios of $\frac{HONO}{NO_x}$ and $\frac{HONO}{NO_2}$ (Table S7 and Figures S17 and S18), and are discussed in detail in the Supporting Information. Overall, a correlation between HONO and NO_2 was observed for experiments conducted with semi-metallic brake pads throughout the entire heavy braking period (r^2 = 0.88 and 0.95 for duplicate experiments). For ceramic brake pads, there was little correlation because of the nonlinearity (r^2 = 0.52 and 0.26) between HONO and NO_2 at the lower NO_2 concentrations, but then a linear increase similar to that for the semi-metallic brake pads at higher NO_2 concentrations (r^2 = 0.90 and 0.98). It is likely that the initial lack of dependence of

https://doi.org/10.1021/acs.est.4c13202
Environ. Sci. Technol. 2025, 59, 9167−9177

HONO on NO_2 at the beginning for ceramic brakes is due to several factors such as lower rotor temperatures (Figures S2, S3), which control both the emissions of species and the kinetics of reactions as discussed in the following paragraphs. In summary, these data clearly show that HONO is directly correlated with NO_2.

Nitrous acid from braking in these experiments could be from direct emissions from the brake pads themselves, such as from the thermal degradation of nitrogen-containing compounds during heating and/or frictional processes, or formed through secondary chemistry occurring within the plume of gases coming off of the brake pads. It has been previously shown that HONO from tailpipe emissions can be generated from reactions of NO_2 with organic gases in diesel combustion exhaust.[75] This was attributed to reaction (R5a), where $\{CH\}_{red}$ represents a group of reduced organics that could be oxidized by NO_2

$$NO_{2(g)} + CH_{red} \rightarrow C_{ox} + HONO \quad \text{(R5a)}$$

It is known that alkenes can react with NO_2 via reversible addition to the double bond, reaction (R5b)[76−79]

$$NO_{2(g)} + RCH = CHR \leftrightarrow RCH(NO_2) - C(.)HR \quad \text{(R5b)}$$

In air, the alkyl radical adds O_2 and undergoes further chemistry to generate stable oxygenated products. A third possibility for reactions with NO_2 is abstraction of a hydrogen atom from an organic compound.

$$NO_{2(g)} + RH \rightarrow R\cdot + HONO_{(g)} \quad \text{(R5c)}$$

Given the strength of typical C−H bonds (∼100 kcal mol^{-1}), this reaction is expected to be slow.[80] However, allylic C−H bonds (C═C−CH) and those in aldehydes (RC(O)−H) are significantly weaker (∼85 kcal mol^{-1}). Formation of HONO by abstraction of allylic hydrogens in lipids was first demonstrated by Pryor and Lightsey.[81] Previous studies of organic gases from braking show a complex suite of semivolatile and volatile organic compounds including many aldehydes as well as alkenes with allylic hydrogens.[62] Notably, higher VOC emissions were also observed by Perraud et al.[62] during the heavy braking conditions compared to lighter braking, as well as for ceramic compared to semi-metallic brakes, both of which are consistent with the higher HONO levels observed during heavy braking and for ceramic brakes in this study. Nitric oxide and NO_2 levels were monitored during these experiments (Figure S16), and high NO_2 levels were reached during heavy braking conditions (up to ∼1800 ppb for ceramic and ∼100 ppb for semi-metallic). In short, reactions between NO_2 and aldehydes and alkenes in brake plumes could be the source of HONO. This is important for the development of control strategies since removal of the organics and NO_x from braking could be more challenging than from exhaust where catalytic converters are very effective.

To investigate whether reaction (R5c) could account for the HONO levels measured during the heavy braking experiments, an experiment was conducted with a sorbent tube containing a standard mixture of alkenes which were desorbed into a heated reaction bulb that contained NO_2. While there was some HONO initially present, likely from heterogeneous NO_2 reactions, HONO increased significantly on addition of the VOC mixture, reaching ∼1000 ppb after 6 min of reaction, equivalent to 7×10^{10} molecules HONO cm^{-3} s^{-1} determined from a linear regression between 0−6 min (Figure 3).

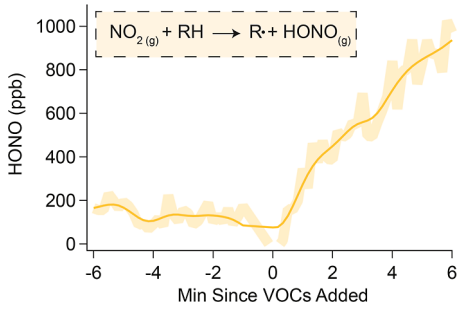

Figure 3. HONO mixing ratios (ppb) from the reaction of 277 ppm of NO_2 with a standard mixture of alkenes at T = 73 °C. Solid line represents smoothed data and shaded region demonstrates variability of data over ∼2 min.

While there is a rich combustion literature on abstraction of hydrogen from compounds such as CH_4 by NO_2, there are relatively few data on allylic hydrogen abstraction by NO_2 and its temperature dependence.[80,82] However, building on the sparse data in the literature,[83−85] a reasonable range of rate constants for allylic hydrogen abstractions could be approximated for temperatures bracketing those at the rotor and in the dynamometer chamber (75 −275 °C). This range of rate constants is quite broad, from 1.4×10^{-20} to 1.5×10^{-16} cm^3 $molecule^{-1}$ s^{-1} depending on the structure of the VOC and the temperature.

Using the measured rate of HONO production (7×10^{10} molecules HONO cm^{-3} s^{-1}), the known NO_2 concentration (7×10^{15} molecules cm^{-3}), and concentrations of VOC that have allylic hydrogen atoms (7×10^{12} molecules cm^{-3}) allows one to estimate the effective reaction rate constant, k^{eff}, from eq 1 as shown below. The value of k^{eff} thus derived is 2×10^{-18} cm^3 $molecules^{-1}$ s^{-1}, in the midrange of the rate constants for allylic hydrogen abstraction based on previous laboratory measurements.[83−85]

$$\frac{d[HONO]}{dt} = k^{eff}[NO_2][VOC] \quad (1)$$

Figure S19 shows an increase in HONO similar to that from the standard mixture when organics from the ceramic and semi-metallic brakes are desorbed into the reaction vessel containing NO_2. To rule out the possibility that HONO increases are attributed to desorption from the sorbent tube, blank experiments were conducted desorbing organic gases collected into a bulb that did not contain NO_2 (Figure S20), which is discussed in detail in the Supporting Information. The sorbent tubes are not 100% efficient in collecting and desorbing all of the VOC emitted by the brakes, such that the VOC concentration will be significantly underestimated, precluding a quantitative analysis. However, these data clearly show that HONO is also generated in the presence of the brake VOC and NO_2 at higher temperatures.

Overall, these results suggest that the HONO generated from the braking experiments included in this study is formed through the reaction of organic gases with NO_2 through (R5c) within the hot plume of gases emitted during braking. An overview of the HONO levels compared to the NO and NO_2 levels, as well as the chamber and rotor temperatures and VOC levels for these experiments is provided in Figures S22−S25 for

https://doi.org/10.1021/acs.est.4c13202
Environ. Sci. Technol. 2025, 59, 9167−9177

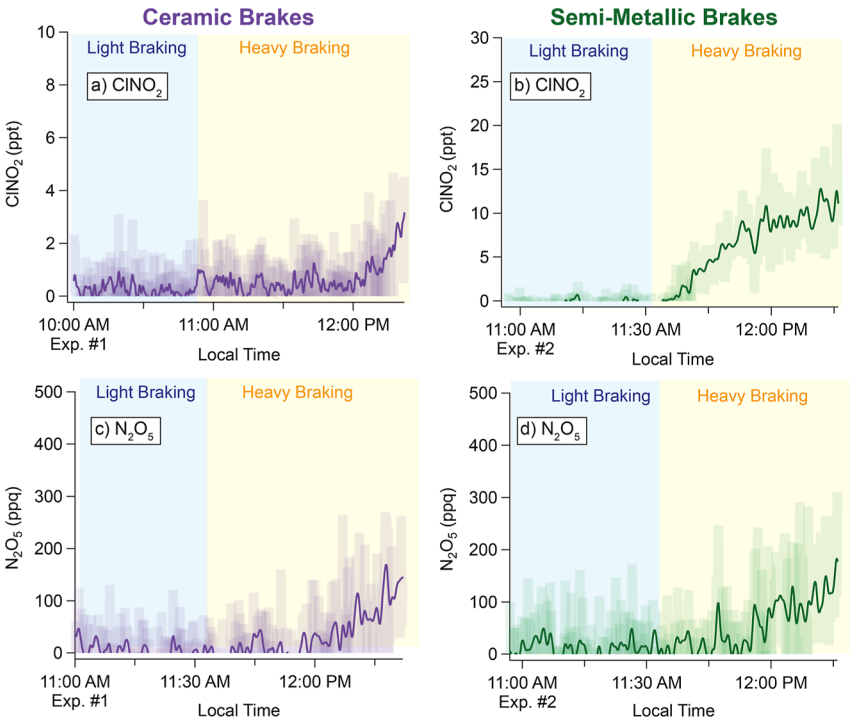

Figure 4. $ClNO_2$ levels during braking experiments using ceramic (4a) and semi-metallic (4b) brake pads. N_2O_5 levels during experiments using ceramic (4c) and semi-metallic (4d) brake pads. Blue region highlights period of light braking conditions and yellow region highlights period of heavy braking conditions. Line on graphs represents smoothed results and shaded region represents the results from ~2 min average of CIMS collection.

experiments 1−4 encompassing both ceramic and semi-metallic brake pads, further demonstrating the role that each of these factors play in HONO formation. This is consistent with the observation of Pitts et al.[23] that HONO was only present in the exhaust of vehicles without a catalytic converter. In that case, formaldehyde and benzaldehyde, which have abstractable hydrogens, were also detected at levels up to ~1 ppm (other organics were not detectable with the DOAS technique that was used).

It is possible that HONO is generated through other pathways during these experiments in addition to (R5c), which could explain the wide range of $\frac{HONO}{NO_2}$ ratio observed (Table S7). Heterogeneous hydrolysis of NO_2 on surfaces, such as the chamber, is also known to form HONO (R4), but this is unlikely to be a significant contributor to the HONO formation in our experiments based on the lack of a trend between chamber RH and HONO, as shown in Figure S21. Additional possible formation mechanisms for HONO include multiphase reactions between NO_2 and black carbon (i.e., graphite). Graphite is a large component of brake pad material,[49,86] and both black carbon and NO_2 have been shown to be emitted during braking processes.[62,66,87] Future studies should be conducted to continue to explore the formation of HONO through braking processes.

$ClNO_2$ and N_2O_5 emissions from braking. In addition to HONO, mixing ratios for $ClNO_2$ and N_2O_5 were quantified throughout the braking experiments. In contrast to HONO, these species were only observed at higher temperatures during heavy braking conditions (Figure 4). For $ClNO_2$, greater overall levels were observed for semi-metallic brakes (Figure 4b) compared to ceramic brakes (Figure 4a). Slightly lower mixing ratios of $ClNO_2$ were observed in the duplicate experiment for ceramic brake pads (Figure S26a), and similar $ClNO_2$ concentrations were measured in the duplicate experiment for semi-metallic brake pads (Figure S26b). The dynamics of $ClNO_2$ generation depended on the brake pad types, with $ClNO_2$ increasing shortly after commencing the heavy braking experiment for semi-metallic pads, but only once reaching the highest temperature conditions after ~30 min of heavy braking for ceramic pads.

Much lower N_2O_5 levels were observed than the other reactive nitrogen gases (Figure 4b,d Figure S26b,d). In addition, N_2O_5 was only observed after ~30 min of heavy braking for both brake pad types. The high temperatures of the rotor and chamber are expected to lead to some thermal decomposition of N_2O_5, which may explain why the N_2O_5 levels are much lower than the other reactive nitrogen species observed in this study. Overall, these results indicate that braking is unlikely to be a significant source of atmospheric N_2O_5, but perhaps is emitted in small quantities under extreme braking conditions.

Like HONO, the N_2O_5 and $ClNO_2$ could be formed through secondary reactions in the expanding plume of gases from the rotor. For example, $ClNO_2$ may form from the multiphase reaction of N_2O_5 with particulate chloride.[88] Future measurements are needed to probe particulate brake emissions for inorganic chloride to explore this pathway as a potential mechanism of $ClNO_2$ formation from automotive braking.

CONCLUSIONS AND ATMOSPHERIC IMPLICATIONS

This study demonstrates that braking processes may lead to emissions of reactive nitrogen species, particularly HONO, at levels sufficient to warrant further investigation of their contribution to ambient air quality. While lower concen-

https://doi.org/10.1021/acs.est.4c13202
Environ. Sci. Technol. 2025, 59, 9167−9177

trations of HONO were observed during the light braking experiments which are more characteristic of day-to-day urban driving conditions, it should be noted that the quantities reported in this study are for one brake pair. Typical passenger vehicles are equipped with four friction brake pairs (one per wheel), and multiplying the quantities observed in these experiments by four results in substantial HONO quantities during light braking conditions. This is certainly an overestimate, as our dynamometer and chamber apparatus do not perfectly simulate real-world driving conditions, and secondary reactions forming HONO will be accelerated at the concentrations in the expanding plume from the brake pads. Additionally, braking forces are ∼80% higher for front-wheels compared to the back-wheels, adding additional uncertainty to this calculation.[89] Nevertheless, the present results indicate that braking processes may be an overlooked contributor to ambient HONO. This is consistent with ambient measurements that suggest HONO sources are near the ground surface[35,36] and remain above detection limits in the daytime despite its short photolysis lifetime.[35] Future experiments, particularly field measurements that monitor HONO levels near roadways or at locations with frequent braking (e.g., traffic stops) are necessary to constrain the contribution of automotive braking to HONO budgets.

Much smaller mixing ratios of $ClNO_2$ and N_2O_5 were measured in this study in comparison to HONO. For over a decade, it has been known that there exists an urban source of $ClNO_2$.[46] It is possible that automotive braking is a minor contributor to ambient $ClNO_2$. Thus, it would be beneficial to conduct further studies into the correlations between urban $ClNO_2$ emissions and traffic patterns.

Given that tailpipe and non-tailpipe emissions are coemitted during vehicle operation, it is possible that field measurements of HONO levels previously attributed to vehicular exhaust could actually be due to a combination of both exhaust and braking emissions. Pitts et al.[23] demonstrated that HONO can be emitted from tailpipe sources lacking a catalytic converter, and subsequently Winer and Biermann[90] measured HONO levels up to 15 ppb in Long Beach, California, noting that HONO correlated well with the primary pollutants CO and NO. From this correlation, they concluded that the HONO was likely from combustion sources. It is possible that non-tailpipe sources may have also contributed since CO and NO are also emitted during braking.[62] Attribution of HONO to ambient braking processes is challenging due to simultaneous emissions from both the tailpipe and non-exhaust emissions during vehicle operation. However, if indeed vehicle braking is a significant source of HONO, it can ultimately result in the degradation of air quality. As vehicle electrification progresses, characterizing and potentially mitigating emissions from non-tailpipe sources will become of increasing concern for the environment and public health. Control of gas phase brake emissions is especially challenging, as, unlike focused tailpipe emissions, the use of catalysts on a diffuse source could be technically problematic.

■ ASSOCIATED CONTENT

Supporting Information

The Supporting Information is available free of charge at https://pubs.acs.org/doi/10.1021/acs.est.4c13202.

Additional experimental details for the braking simulations are provided, including Table S1, listing all experiments included in this study, and Figures S1−S3, presenting the braking conditions (braking pressure, torque, rotor temperature, and chamber temperature) for the additional experiments included in this study. Details regarding the operation of the CIMS during the experiments are discussed, and further details are provided regarding the calibration of the CIMS for the reactive nitrogen species. A diagram is provided for the HONO calibration apparatus in Figure S4. Table S2 includes details regarding the HONO and dilution flows, HONO mixing ratio, and CIMS signal for all calibration points. Results from control experiments conducted to assess the stability of the HONO generation system are presented in Figure S5, and example FTIR spectra utilized to determine the stable mixing ratio of HONO are included in Figure S6. Details of the synthesis of N_2O_5 and $ClNO_2$ standards are described, and a diagram of the online calibration delivery system for $ClNO_2$ and N_2O_5 is provided in Figure S7. An example of the linear regression of signal decay during the calibration procedure for these analytes is provided in Figure S8. Tables S3 and S4 provide details for the analyte flows, dilution flows, analyte mixing ratio, and CIMS signal response for N_2O_5 and $ClNO_2$ calibrations. The results of the calibration of CIMS for HONO, N_2O_5, and $ClNO_2$ are provided in Figure S9. A comparison of the CIMS response factor for $ClNO_2$ and N_2O_5 is shown in Figure S10. Details regarding the control experiments reacting organic gases with NO_2 are discussed, and the composition of organic gases collected on the sorbent tubes for these experiments is presented in Tables S5 − S6. Results from the duplicate experiments are discussed. HONO mixing ratios from the duplicate experiments are presented in Figure S11. The relationship of $T_{chamber}$ and T_{rotor} with HONO levels is shown in Figures S12−S15. Measurements of NO and NO_2 are discussed and presented in Figure S16. A summary of the ratios of $\frac{HONO}{NO_x}$ and $\frac{HONO}{NO_2}$ for all heavy braking experiments is discussed. Details for the ratios are presented in Table S6 and in Figure S17. A linear regression for NO_2 vs HONO for all experiments is shown in Figure S18. The estimation of HONO formation from the reaction of NO_2 with organic gases is discussed in detail. The results of control experiments reacting gases collected during heavy braking with NO_2 is presented in Figure S19. Blank experiments of organic gases from heavy braking periods in the absence of NO_2 are included in Figure S20. A comparison of chamber RH and HONO levels is included in Figure S21. An overview of HONO levels compared to braking and rotor temperatures, NO_x concentrations, and VOC levels is discussed and presented for all experiments in Figures S22−S25. $ClNO_2$ and N_2O_5 mixing ratios from the duplicate experiments are presented in Figure S26 (PDF).

■ AUTHOR INFORMATION

Corresponding Authors

Barbara J. Finlayson-Pitts − *Department of Chemistry, University of California Irvine, Irvine, California 92697, United States;* orcid.org/0000-0003-4650-168X; Email: bjfinlay@uci.edu

https://doi.org/10.1021/acs.est.4c13202
Environ. Sci. Technol. 2025, 59, 9167−9177

James N. Smith − *Department of Chemistry, University of California Irvine, Irvine, California 92697, United States;* orcid.org/0000-0003-4677-8224; Email: jimsmith@uci.edu

Authors

Madeline E. Cooke − *Department of Chemistry, University of California Irvine, Irvine, California 92697, United States;* orcid.org/0000-0003-0955-0351

Michelia Dam − *Department of Chemistry, University of California Irvine, Irvine, California 92697, United States*

Lisa M. Wingen − *Department of Chemistry, University of California Irvine, Irvine, California 92697, United States;* orcid.org/0000-0001-5847-9913

Véronique Perraud − *Department of Chemistry, University of California Irvine, Irvine, California 92697, United States;* orcid.org/0000-0003-1247-9787

Adam E. Thomas − *Department of Chemistry, University of California Irvine, Irvine, California 92697, United States*

Berenice Rojas − *Department of Chemistry, University of California Irvine, Irvine, California 92697, United States*

Sanjeevi Nagalingam − *Department of Chemistry, University of California Irvine, Irvine, California 92697, United States;* orcid.org/0000-0003-2520-5742

Michael J. Ezell − *Department of Chemistry, University of California Irvine, Irvine, California 92697, United States*

Samuel La Salle − *Department of Chemistry, University of California Irvine, Irvine, California 92697, United States*

Paulus S. Bauer − *Department of Chemistry, University of California Irvine, Irvine, California 92697, United States*

Complete contact information is available at: https://pubs.acs.org/10.1021/acs.est.4c13202

Notes

The authors declare no competing financial interest.

■ ACKNOWLEDGMENTS

This research was supported by the California Department of Justice (no. AERTF-221620) and National Science Foundation (no. 2327825). This material is based upon work supported by the National Science Foundation under Award no. 2324901. The authors would like to gratefully acknowledge Mark Steinborn and Shane Embleton of the UCI machine shop for their support in the operation of the dynamometer for the braking simulations presented herein.

■ ABBREVIATIONS

(VOC), volatile organic compound; (NO_x), nitrogen oxides; (SOA), secondary organic aerosol; (CIMS), chemical ionization mass spectrometry; (HONO), nitrous acid; ($ClNO_2$), nitryl chloride; (N_2O_5), dinitrogen pentoxide; (NO_2), nitrogen dioxide; (NO), nitric oxide; (CO), carbon monoxide

■ REFERENCES

(1) Finlayson-Pitts, B. J.; Pitts, J. N. *Chemistry of the Upper and Lower Atmosphere*; Academic Press: San Diego, CA, 2000.

(2) Finlayson-Pitts, B. J. Introductory lecture: atmospheric chemistry in the Anthropocene. *Faraday Discuss.* **2017**, *200*, 11−58.

(3) Spataro, F.; Ianniello, A. Sources of atmospheric nitrous acid: State of the science, current research needs, and future prospects. *J. Air Waste Manage. Assoc.* **2014**, *64* (11), 1232−1250.

(4) Elshorbany, Y. F.; Kurtenbach, R.; Wiesen, P.; Lissi, E.; Rubio, M.; Villena, G.; Gramsch, E.; Rickard, A. R.; Pilling, M. J.; Kleffmann, J. Oxidation capacity of the city air of Santiago, Chile. *Atmos. Chem. Phys.* **2009**, *9* (6), 2257−2273.

(5) Michoud, V.; Kukui, A.; Camredon, M.; Colomb, A.; Borbon, A.; Miet, K.; Aumont, B.; Beekmann, M.; Durand-Jolibois, R.; Perrier, S.; Zapf, P.; Siour, G.; Ait-Helal, W.; Locoge, N.; Sauvage, S.; Afif, C.; Gros, V.; Furger, M.; Ancellet, G.; Doussin, J. F. Radical budget analysis in a suburban European site during the MEGAPOLI summer field campaign. *Atmos. Chem. Phys.* **2012**, *12* (24), 11951−11974.

(6) Acker, K.; Febo, A.; Trick, S.; Perrino, C.; Bruno, P.; Wiesen, P.; Möller, D.; Wieprecht, W.; Auel, R.; Giusto, M.; Geyer, A.; Platt, U.; Allegrini, I. Nitrous acid in the urban area of Rome. *Atmos. Environ.* **2006**, *40* (17), 3123−3133.

(7) Osthoff, H. D.; Roberts, J. M.; Ravishankara, A. R.; Williams, E. J.; Lerner, B. M.; Sommariva, R.; Bates, T. S.; Coffman, D.; Quinn, P. K.; Dibb, J. E.; Stark, H.; Burkholder, J. B.; Talukdar, R. K.; Meagher, J.; Fehsenfeld, F. C.; Brown, S. S. High levels of nitryl chloride in the polluted subtropical marine boundary layer. *Nat. Geosci* **2008**, *1* (5), 324−328.

(8) Cai, X.; Griffin, R. J. Secondary aerosol formation from the oxidation of biogenic hydrocarbons by chlorine atoms. *J. Geophys. Res. Atmos.* **2006**, *111* (D14), D14206.

(9) Dhulipala, S. V.; Bhandari, S.; Hildebrandt Ruiz, L. Formation of oxidized organic compounds from Cl-initiated oxidation of toluene. *Atmos. Environ.* **2019**, *199*, 265−273.

(10) Finlayson-Pitts, B. J.; Ezell, M. J.; Pitts Jr, J. N. Formation of chemically active chlorine compounds by reactions of atmospheric NaCl particles with gaseous N_2O_5 and $ClONO_2$. *Nature* **1989**, *337* (19), 241−244.

(11) Tham, Y. J.; Wang, Z.; Li, Q.; Wang, W.; Wang, X.; Lu, K.; Ma, N.; Yan, C.; Kecorius, S.; Wiedensohler, A.; Zhang, Y.; Wang, T. Heterogeneous N_2O_5 uptake coefficient and production yields of $ClNO_2$ in polluted northern China: Roles of aerosol water content and chemical composition. *Atmos. Chem. Phys.* **2018**, *18*, 13155−13171.

(12) Wang, Z.; Wang, W.; Tham, Y. J.; Li, Q.; Wang, H.; Wen, L.; Wang, X.; Wang, T. Fast heterogeneous N_2O_5 uptake and $ClNO_2$ production in power plant and industrial plumes observed in the nocturnal residual layer over the north China plain. *Atmos. Chem. Phys.* **2017**, *17*, 12361−12378.

(13) Burkholder, J. B.; P. S, S.; Abbatt, J.; Barker, J. R.; Cappa, C.; Crounse, J. D.; Dibble, T. S.; Huie, R. E.; Kolb, C. E.; Kurylo, M. J.; O, V. L.; Percival, C. J.; Wilmouth, D. M.; Wine, P. H. Chemical Kinetics and Photochemical Data for Use in Atmospheric Studies.JPL Publication 19−5; Laboratory, J. P., Ed.; Pasadena, 2019.

(14) Ammann, M.; Cox, R. A.; Crowley, J. N.; Jenkin, M. E.; Mellouki, A.; Rossi, M. J.; Troe, J.; Wallington, T. J. Evaluated kinetic and photochemical data for atmospheric chemistry: Volume VI − heterogeneous reactions with liquid substrates. *Atmos. Chem. Phys.* **2013**, *13* (16), 8045−8228.

(15) Crowley, J. N.; Ammann, M.; Cox, R. A.; Hynes, R. G.; Jenkin, M. E.; Mellouki, A.; Rossi, M. J.; Troe, J.; Wallington, T. J. Corrigendum to ″Evaluated kinetic and photochemical data for atmospheric chemistry: Volume V − heterogeneous reactions on solid substrates″ published in Atmos. *Chem. Phys.* **2010**, *10*, 9059−9223.

(16) Crowley, J. N.; Ammann, M.; Cox, R. A.; Hynes, R. G.; Jenkin, M. E.; Mellouki, A.; Rossi, M. J.; Troe, J.; Wallington, T. J. Evaluated kinetic and photochemical data for atmospheric chemistry: Volume V − heterogeneous reactions on solid substrates. *Atmos. Chem. Phys.* **2010**, *10* (18), 9059−9223.

(17) Platt, U.; Perner, D.; Harris, G. W.; Winer, A. M.; Pitts, J. N. Observations of nitrous acid in the urban atmosphere by differential optical absorption. *Nature* **1980**, *285*, 312−314.

(18) Perner, D.; Platt, U. Detection of nitrous acid in the atmosphere by differential optical absorption. *Geophys. Res. Lett.* **1979**, *6* (12), 917−920.

(19) Wang, X.; Li, D.; Flaud, P.-M.; Li, H.; Perrier, S.; Villenave, E.; Dusanter, S.; Tomas, A.; Perraudin, E.; George, C.; Riva, M. Atmospheric nitrous acid measurement in the french landes forest. *ACS Earth Space Chem.* **2022**, *6* (1), 25−33.

(20) Kleffmann, J.; Gavriloaiei, T.; Hofzumahaus, A.; Holland, F.; Koppmann, R.; Rupp, L.; Schlosser, E.; Siese, M.; Wahner, A. Daytime formation of nitrous acid: A major source of OH radicals in a forest. *Geophys. Res. Lett.* **2005**, *32* (5), L05818..
(21) Meusel, H.; Kuhn, U.; Reiffs, A.; Mallik, C.; Harder, H.; Martinez, M.; Schuladen, J.; Bohn, B.; Parchatka, U.; Crowley, J. N.; Fischer, H.; Tomsche, L.; Novelli, A.; Hoffmann, T.; Janssen, R. H. H.; Hartogensis, O.; Pikridas, M.; Vrekoussis, M.; Bourtsoukidis, E.; Weber, B.; Lelieveld, J.; Williams, J.; Pöschl, U.; Cheng, Y.; Su, H. Daytime formation of nitrous acid at a coastal remote site in Cyprus indicating a common ground source of atmospheric HONO and NO. *Atmos. Chem. Phys.* **2016**, *16*, 14475−14493.
(22) Zhong, X.; Shen, H.; Zhao, M.; Zhang, J.; Sun, Y.; Liu, Y.; Zhang, Y.; Shan, Y.; Li, H.; Mu, J.; Yang, Y.; Nie, Y.; Tang, J.; Dong, C.; Wang, X.; Zhu, Y.; Guo, M.; Wang, W.; Xue, L. Nitrous acid budgets in the coastal atmosphere: potential daytime marine sources. *Atmos. Chem. Phys.* **2023**, *23*, 14761−14778.
(23) Pitts, J. N.; Biermann, H. W.; Winer, A. M.; Tuazon, E. C. Spectroscopic identification and measurement of gaseous nitrous acid in dilute auto exhaust. *Atmos. Environ.* **1984**, *18* (4), 847−854.
(24) Theys, N.; Volkamer, R.; Müller, J. F.; Zarzana, K. J.; Kille, N.; Clarisse, L.; De Smedt, I.; Lerot, C.; Finkenzeller, H.; Hendrick, F.; Koenig, T. K.; Lee, C. F.; Knote, C.; Yu, H.; Van Roozendael, M. Global nitrous acid emissions and levels of regional oxidants enhanced by wildfires. *Nat. Geosci* **2020**, *13* (10), 681−686.
(25) George, C.; Strekowski, R. S.; Kleffmann, J.; Stemmler, K.; Ammann, M. Photoenhanced uptake of gaseous NO_2 on solid organic compounds: a photochemical source of HONO? *Faraday Discuss.* **2005**, *130*, 195−210.
(26) Ye, C.; Zhang, N.; Gao, H.; Zhou, X. Photolysis of Particulate Nitrate as a Source of HONO and NO(x). *Environ. Sci. Technol.* **2017**, *51* (12), 6849−6856.
(27) Ye, C.; Gao, H.; Zhang, N.; Zhou, X. Photolysis of nitric acid and nitrate on natural and artificial surfaces. *Environ. Sci. Technol.* **2016**, *50* (7), 3530.
(28) Su, H.; Cheng, Y.; Oswald, R.; Behrendt, T.; Trebs, I.; Meixner, F. X.; Andreae, M. O.; Cheng, P.; Zhang, Y.; Pöschl, U. Soil nitrite as a source of atmospheric HONO and OH radicals. *Science* **2011**, *333*, 1616−1618.
(29) Donaldson, M. A.; Bish, D. L.; Raff, J. D. Soil surface acidity plays a determining role in the atmospheric-terrestrial exchange of nitrous acid. *Proc. Natl. Acad. Sci. U.S.A.* **2014**, *111* (52), 18472−18477.
(30) Scharko, N. K.; Schutte, U. M.; Berke, A. E.; Banina, L.; Peel, H. R.; Donaldson, M. A.; Hemmerich, C.; White, J. R.; Raff, J. D. Combined flux chamber and genomics approach links nitrous acid emissions to ammonia oxidizing bacteria and archaea in urban and agricultural soil. *Environ. Sci. Technol.* **2015**, *49* (23), 13825−13834.
(31) Finlayson-Pitts, B. J.; Wingen, L. M.; Sumner, A. L.; Syomin, D.; Ramazan, K. A. The heterogeneous hydrolysis of NO_2 in laboratory systems and in outdoor and indoor atmospheres: An integrated mechanism. *Phys. Chem. Chem. Phys.* **2003**, *5* (2), 223−242.
(32) Gustafsson, R. J.; Orlov, A.; Griffiths, P. T.; Cox, R. A.; Lambert, R. M. Reduction of NO_2 to nitrous acid on illuminated titanium dioxide aerosol surfaces: implications for photocatalysis and atmospheric chemistry. *Chem. Commun. (Camb)* **2006**, *37*, 3936.
(33) Stutz, J.; Alicke, B.; Ackermann, R.; Geyer, A.; Wang, S.; White, A. B.; Williams, E. J.; Spicer, C. W.; Fast, J. D. Relative humidity dependence of HONO chemistry in urban areas. *J. Geophys. Res. Atmos.* **2004**, *109* (D3), D03307..
(34) Calvert, J. G.; Yarwood, G.; Dunker, A. M. An evaluation of the mechanism of nitrous acid formation in the urban atmosphere. *Res. Chem. Intermed.* **1994**, *20*, 463−502.
(35) VandenBoer, T. C.; Brown, S. S.; Murphy, J. G.; Keene, W. C.; Young, C. J.; Pszenny, A. A. P.; Kim, S.; Warneke, C.; de Gouw, J. A.; Maben, J. R.; Wagner, N. L.; Riedel, T. P.; Thornton, J. A.; Wolfe, D. E.; Dubé, W. P.; Öztürk, F.; Brock, C. A.; Grossberg, N.; Lefer, B.; Lerner, B.; Middlebrook, A. M.; Roberts, J. M. Understanding the role of the ground surface in HONO vertical structure: High resolution vertical profiles during NACHTT-11. *J. Geophys. Res. Atmos.* **2013**, *118* (17), 10155−10171.
(36) Wong, K. W.; Tsai, C.; Lefer, B.; Haman, C.; Grossberg, N.; Brune, W. H.; Ren, X.; Luke, W.; Stutz, J. Daytime HONO vertical gradients during SHARP 2009 in Houston, TX. *Atmos. Chem. Phys.* **2012**, *12* (2), 635−652.
(37) Yang, W.; Han, C.; Zhang, T.; Tang, N.; Yang, H.; Xue, X. Heterogeneous photochemical uptake of NO_2 on the soil surface as an important ground-level HONO source. *Environ. Pollut.* **2021**, *271*, 116289.
(38) Stemmler, K.; Ammann, M.; Donders, C.; Kleffmann, J.; George, C. Photosensitized reduction of nitrogen dioxide on humic acid as a source of nitrous acid. *Nature* **2006**, *440* (7081), 195−198.
(39) Mothes, F.; Hoffmann, E. H.; Herrmann, H. Urban grime photochemistry and its interaction with air pollutants NO, NO_2, and O_3: A aource for HONO and NO_2 impacting OH in urban areas. *ACS Earth Space Chem.* **2023**, *7* (11), 2263−2274.
(40) Liu, J.; Li, B.; Deng, H.; Yang, Y.; Song, W.; Wang, X.; Luo, Y.; Francisco, J. S.; Li, L.; Gligorovski, S. Resolving the Formation Mechanism of HONO via Ammonia-Promoted Photosensitized Conversion of Monomeric NO_2 on Urban Glass Surfaces. *J. Am. Chem. Soc.* **2023**, *145* (21), 11488−11493.
(41) Liu, J.; Li, S.; Mekic, M.; Jiang, H.; Zhou, W.; Loisel, G.; Song, W.; Wang, X.; Gligorovski, S. Photoenhanced Uptake of NO_2 and HONO Formation on Real Urban Grime. *Environ. Sci. Technol. Lett* **2019**, *6* (7), 413−417.
(42) Riedel, T. P.; Bertram, T. H.; Crisp, T. A.; Williams, E. J.; Lerner, B. M.; Vlasenko, A.; Li, S. M.; Gilman, J.; de Gouw, J.; Bon, D. M.; Wagner, N. L.; Brown, S. S.; Thornton, J. A. Nitryl chloride and molecular chlorine in the coastal marine boundary layer. *Environ. Sci. Technol.* **2012**, *46* (19), 10463−10470.
(43) Hall, R.; Nepotchatykh, O.; Nepotchatykh, E.; Ariya, P. A. Anthropogenic photolabile chlorine in the cold-climate city of Montreal. *Atmosphere* **2020**, *11* (8), 812.
(44) Mielke, L. H.; Furgeson, A.; Odame-Ankrah, C. A.; Osthoff, H. D. Ubiquity of $ClNO_2$ in the urban boundary layer of Calgary, Alberta, Canada. *Can. J. Chem.* **2016**, *94* (4), 414−423.
(45) McNamara, S. M.; Kolesar, K. R.; Wang, S.; Kirpes, R. M.; May, N. W.; Gunsch, M. J.; Cook, R. D.; Fuentes, J. D.; Hornbrook, R. S.; Apel, E. C.; China, S.; Laskin, A.; Pratt, K. A. Observation of road salt aerosol driving inland wintertime atmospheric chlorine chemistry. *ACS Cent. Sci.* **2020**, *6* (5), 684−694.
(46) Mielke, L. H.; Furgeson, A.; Osthoff, H. D. Observation of $ClNO_2$ in a mid-continental urban environment. *Environ. Sci. Technol.* **2011**, *45* (20), 8889−8896.
(47) Atkinson, R.; Winer, A. M.; Pitts, J. N. Estimation of nighttime N_2O_5 concentrations from ambient NO_2 and NO_3 radical concentrations and the role of N_2O_5 in nighttime chemistry. *Atmos. Environ.* **1986**, *20*, 331−339.
(48) Chang, W. L.; Bhave, P. V.; Brown, S. S.; Riemer, N.; Stutz, J.; Dabdub, D. Heterogeneous atmospheric chemistry, ambient measurements, and model calculations of N_2O_5: A Review. *Aerosol Sci. Technol.* **2011**, *45* (6), 665−695.
(49) Thorpe, A.; Harrison, R. M. Sources and properties of non-exhaust particulate matter from road traffic: a review. *Sci. Total Environ.* **2008**, *400* (1−3), 270−282.
(50) Piscitello, A.; Bianco, C.; Casasso, A.; Sethi, R. Non-exhaust traffic emissions: Sources, characterization, and mitigation measures. *Sci. Total Environ.* **2021**, *766*, 144440.
(51) Fussell, J. C.; Franklin, M.; Green, D. C.; Gustafsson, M.; Harrison, R. M.; Hicks, W.; Kelly, F. J.; Kishta, F.; Miller, M. R.; Mudway, I. S.; Oroumiyeh, F.; Selley, L.; Wang, M.; Zhu, Y. A review of road traffic-derived non-exhaust particles: Emissions, physicochemical characteristics, health risks, and mitigation measures. *Environ. Sci. Technol.* **2022**, *56* (11), 6813−6835.
(52) zum Hagen, F. H. F.; Mathissen, M.; Grabiec, T.; Hennicke, T.; Rettig, M.; Grochowicz, J.; Vogt, R.; Benter, T. Study of brake wear

https://doi.org/10.1021/acs.est.4c13202
Environ. Sci. Technol. 2025, 59, 9167−9177

particle emissions: Impact of braking and cruising conditions. *Environ. Sci. Technol.* **2019**, *53* (9), 5143−5150.
(53) Farwick zum Hagen, F. H.; Mathissen, M.; Grabiec, T.; Hennicke, T.; Rettig, M.; Grochowicz, J.; Vogt, R.; Benter, T. On-road vehicle measurements of brake wear particle emissions. *Atmos. Environ.* **2019**, *217*, 116943.
(54) Zhao, J.; Lewinski, N.; Riediker, M. Physico-chemical characterization and oxidative reactivity evaluation of aged brake wear particles. *Aerosol Sci. Technol.* **2015**, *49* (2), 65−74.
(55) Thomas, A. E.; Bauer, P. S.; Dam, M.; Perraud, V.; Wingen, L. M.; Smith, J. N. Automotive braking is a source of highly charged aerosol particles. *Proc. Natl. Acad. Sci. U.S.A.* **2024**, *121* (13), No. e2313897121.
(56) Sanders, P. G.; Xu, N.; Dalka, T. M.; Maricq, M. M. Airborne brake wear debris: Size distributions, composition, and a comparison of dynamometer and vehicle tests. *Environ. Sci. Technol.* **2003**, *37* (18), 4060−4069.
(57) Kukutschova, J.; Moravec, P.; Tomasek, V.; Matejka, V.; Smolik, J.; Schwarz, J.; Seidlerova, J.; Safarova, K.; Filip, P. On airborne nano/micro-sized wear particles released from low-metallic automotive brakes. *Environ. Pollut.* **2011**, *159* (4), 998−1006.
(58) Kukutschová, J.; Filip, P. Review of brake wear emissions. *Non-Exhaust Emissions* **2018**, 123−146.
(59) Mathissen, M.; Grigoratos, T.; Lahde, T.; Vogt, R. Brake wear particle emissions of a passenger car measured on a chassis dynamometer. *Atmosphere* **2019**, *10* (9), 556.
(60) Nosko, O.; Vanhanen, J.; Olofsson, U. Emission of 1.3−10 nm airborne particles from brake materials. *Aerosol Sci. Technol.* **2017**, *51* (1), 91−96.
(61) Nosko, O.; Olofsson, U. Effective density of airborne wear particles from car brake materials. *J. Aerosol Sci.* **2017**, *107*, 94−106.
(62) Perraud, V.; Blake, D. R.; Wingen, L. M.; Barletta, B.; Bauer, P. S.; Campos, J.; Ezell, M. J.; Guenther, A.; Johnson, K. N.; Lee, M.; Meinardi, S.; Patterson, J.; Saltzman, E. S.; Thomas, A. E.; Smith, J. N.; Finlayson-Pitts, B. J. Unrecognized volatile and semi-volatile organic compounds from brake wear. *Environmental Science: Processes & Impacts* **2024**, *26* (5), 928−941.
(63) Patel, A.; Aggarwal, S.; Bard, L.; Durif, O.; Introna, M.; Juarez-Facio, A. T.; Tu, M.; Elihn, K.; Noziere, B.; Olofsson, U.; Steimer, S. S. Gaseous emissions from brake wear can form secondary particulate matter. *Sci. Rep.* **2024**, *14* (1), 23253.
(64) Chan, D.; Stachowiak, G. W. Review of automotive brake friction materials. *Proc. Inst. Mech. Eng* **2004**, *218* (9), 953−966.
(65) Borawski, A. Testing passenger car brake pad exploitation time's impact on the values of the coefficient of friction and abrasive wear rate using a pin-on-disc method. *Materials* **2022**, *15* (6), 1991.
(66) Fang, T.; Kapur, S.; Edwards, K. C.; Hagino, H.; Wingen, L. M.; Perraud, V.; Thomas, A. E.; Bliss, B.; Herman, D. A.; De Vizcaya Ruiz, A.; Kleinman, M. T.; Smith, J. N.; Shiraiwa, M. Aqueous OH radical production by brake wear particles. *Environ. Sci. Technol. Lett* **2024**, *11* (4), 315−322.
(67) Stanard, A.; DeFries, T.; Palacios, C.; Kishan, S., *Brake and Tire Wear Emissions Project 17RD016*; Eastern Research Group; 2021.
(68) Tutuianu, M.; Bonnel, P.; Ciuffo, B.; Haniu, T.; Ichikawa, N.; Marotta, A.; Pavlovic, J.; Steven, H. Development of the world-wide harmonized light duty test cycle (WLTC) and a possible pathway for its introduction in the European legislation. *Transp. Res. D: Transp. Environ* **2015**, *40*, 61−75.
(69) Niemann, H.; Winner, H.; Asbach, C.; Kaminski, H.; Zessinger, M. *System Identification Method for Brake Particle Emission Measurements of Passenger Car Disc Brakes on a Dynamometer*; SAE Technical Paper Series, 2018; pp 1−9.
(70) Dunlea, E. J.; Herndon, S. C.; Nelson, D. D.; Volkamer, R. M.; San Martini, F.; Sheehy, P. M.; Zahniser, M. S.; Shorter, J. H.; Wormhoudt, J. C.; Lamb, B. K.; Allwine, E. J.; Gaffney, J. S.; Marley, N. A.; Grutter, M.; Marquez, C.; Blanco, S.; Cardenas, B.; Retama, A.; Ramos Villegas, C. R.; Kolb, C. E.; Molina, L. T.; et al. Evaluation of nitrogen dioxide chemiluminescence monitors in a polluted urban environment. *Atmos. Chem. Phys.* **2007**, *7*, 2691−2704.
(71) Li, X.; Chee, S.; Hao, J.; Abbatt, J. P. D.; Jiang, J.; Smith, J. N. Relative humidity effect on the formation of highly oxidized molecules and new particles during monoterpene oxidation. *Atmos. Chem. Phys.* **2019**, *19* (3), 1555−1570.
(72) Syomin, D. A.; Finlayson-Pitts, B. J. HONO decomposition on borosilicate glass surfaces: implications for environmental chamber studies and field experiments. *Phys. Chem. Chem. Phys.* **2003**, *5* (23), 5236−5242.
(73) Wingen, L. M.; Barney, W. S.; Lakin, M. J.; Brauers, T.; Finlayson-Pitts, B. J. A unique method for laboratory quantification of gaseous nitrous acid (HONO) using the reaction HONO + HCl -> ClNO + H_2O. *J. Phys. Chem. A* **2000**, *104*, 329−335.
(74) Iyer, S.; Lopez-Hilfiker, F.; Lee, B. H.; Thornton, J. A.; Kurten, T. Modeling the detection of organic and inorganic compounds using iodide-based chemical ionization. *J. Phys. Chem. A* **2016**, *120* (4), 576−587.
(75) Gutzwiller, L.; Arens, F.; Baltensperger, U.; Gäggeler, H. W.; Ammann, M. Significance of semivolatile diesel exhaust organics for secondary HONO formation. *Environ. Sci. Technol.* **2002**, *36*, 677−682.
(76) Atkinson, R.; Aschmann, S. M.; Winer, A. M.; Pitts, J. N. Gas phase reaction of NO_2 with alkenes and dialkenes. *Int. J. Chem. Kinet.* **1984**, *16* (6), 697−706.
(77) Bernard, F.; Cazaunau, M.; Mu, Y.; Wang, X.; Daele, V.; Chen, J.; Mellouki, A. Reaction of NO2 with selected conjugated alkenes. *J. Phys. Chem. A* **2013**, *117* (51), 14132−14140.
(78) Sprung, J. L.; Akimoto, H.; Pitts, J. N. Nitrogen dioxide catalyzed geometric isomerization of olefins. Isomerization kinetics of the 2-butenes and 2-pentenes. *J. Am. Chem. Soc.* **1974**, *96* (21), 6549−6554.
(79) Ohta, T.; Nagura, H.; Suzuki, S. Rate constants for the reactions of conjugated olefins with NO_2 in the gas phase. *Int. J. Chem. Kinet.* **1986**, *18* (1), 1−11.
(80) Slack, M. W.; Grillo, A. R. Shock Tube Investigation of Methane-Oxygen Ignition Sensitized by NO_2. *Combust. Flame* **1981**, *40*, 155−172.
(81) Pryor, W. A.; Lightsey, J. W. Mechanisms of nitrogen dioxide reactions: Initiation of lipid peroxidation and the production of nitrous acid. *Science* **1981**, *214*, 435−437.
(82) Chai, J.; Goldsmith, C. F. Rate coefficients for fuel + NO2: Predictive kinetics for HONO and HNO2 formation. *Proc. Combust. Inst.* **2017**, *36* (1), 617−626.
(83) Huie, R. E. The Reaction Kinetics of NO_2. *Toxicology* **1994**, *89*, 193−216.
(84) Jaffe, S. W.; Wan, E. Thermal and photochemical reactions of NO_2 with butyraldehyde in gas phase. *Environ. Sci. Technol.* **1974**, *8* (12), 1024−1025.
(85) Davis, A. M.; Corcoran, W. H. Rate and mechanism of the partial oxidation of acetaldehyde by parts-per-million concentrations of nitrogen dioxide. *Ind. Eng. Chem. Fundam.* **1972**, *11* (4), 431−439.
(86) Borawski, A. Conventional and unconventional materials used in the production of brake pads − review. *Sci. Eng. Compos. Mater* **2020**, *27* (1), 374−396.
(87) Lyu, Y.; Olofsson, U. On black carbon emission from automotive disc brakes. *J. Aerosol Sci.* **2020**, *148*, 105610.
(88) Livingston, F. E.; Finlayson-Pitts, B. J. The reaction of gaseous N_2O_5 with solid NaCl at 298 K: Estimated lower limit to the reaction probability and its potential role in tropospheric and stratospheric chemistry. *Geophys. Res. Lett.* **1991**, *18* (1), 17−20.
(89) Iijima, A.; Sato, K.; Yano, K.; Kato, M.; Kozawa, K.; Furuta, N. Emission factor for antimony in brake abrasion dusts as one of the major atmospheric antimony sources. *Environ. Sci. Technol.* **2008**, *42*, 2937−2942.
(90) Winer, A. M.; Biermann, H. W. Long path differential optical absorption spectroscopy (DOAS) measurements of gaseous HONO, NO_2, and HCHO in the California south coast air basin. *Res. Chem. Intermed.* **1994**, *20*, 423−445.

https://doi.org/10.1021/acs.est.4c13202
Environ. Sci. Technol. 2025, 59, 9167−9177

NOTE ADDED AFTER ASAP PUBLICATION

Due to a production error, the version of this paper that was published ASAP April 30, 2025, contained formatting errors in eqs R2 and R3. The corrected version was posted April 30, 2025.

https://doi.org/10.1021/acs.est.4c13202
Environ. Sci. Technol. 2025, 59, 9167−9177